

1 **Controls on Lunar Basaltic Volcanic Eruption Structure and Morphology:**
2 **Gas Release Patterns in Sequential Eruption Phases**

3 **L. Wilson^{1,2} and J. W. Head²**

4 ¹Lancaster Environment Centre, Lancaster University, Lancaster LA1 4YQ, UK

5 ²Department of Earth, Environmental and Planetary Sciences, Brown University, Providence, RI
6 02912 USA

7
8 **Key Points:**

- 9 • Relationships between a diverse array of lunar mare effusive and explosive volcanic
10 deposits and landforms have previously been poorly understood.
- 11 • Four stages in the generation, ascent and eruption of magma and gas release patterns are
12 identified and characterized.
- 13 • Specific effusive, explosive volcanic deposits and landforms are linked to these four
14 stages in lunar mare basalt eruptions in a predictive and integrated manner.
15

16 **Abstract**

17 Assessment of mare basalt gas release patterns during individual eruptions provides the basis for
18 predicting the effect of vesiculation processes on the structure and morphology of associated
19 features. We subdivide typical lunar eruptions into four phases: *Phase 1*, dike penetrates to the
20 surface, transient gas release phase; *Phase 2*, dike base still rising, high flux hawaiian eruptive
21 phase; *Phase 3*, dike equilibration, lower flux hawaiian to strombolian transition phase; *Phase 4*,
22 dike closing, strombolian vesicular flow phase. We show how these four phases of mare basalt
23 volatile release, together with total dike volumes, initial magma volatile content, vent
24 configuration and magma discharge rate, can help relate the wide range of apparently disparate
25 lunar volcanic features (pyroclastic mantles, small shield volcanoes, compound flow fields,
26 sinuous rilles, long lava flows, pyroclastic cones, summit pit craters, irregular mare patches
27 (IMPs) and ring moat dome structures (RMDSs)) to a common set of eruption processes.

28

29 **Plain Language Summary**

30 Since the early days of close-up orbital observations of the lunar surface in the 1960s, a large
31 number of lunar volcanic landforms have been identified and cataloged, including explosive
32 volcanic mantles, small shield-shaped volcanoes, compound flow fields, meandering sinuous
33 rille channels, long lava flows, volcanic cones, volcanic pit craters, and very unusual and
34 enigmatic features called irregular mare patches (IMPs) and ring moat dome structures
35 (RMDSs). Unknown is how all of these different features form and how they might fit together
36 in different stages or phases of lunar volcanic eruptions. Interpretation is complicated by the
37 effects of low lunar gravity and lack of an atmosphere, both encouraging very different patterns
38 of gas release during lunar volcanic eruptions. We examine the nature of the rise, eruption and
39 gas release of lavas from the lunar interior, and show how four phases of mare basalt eruptions
40 can help relate the wide range of apparently disparate lunar volcanic features to a common set of
41 eruption processes. This is important because it links the observed geologic record to specific
42 physical volcanology predictions that can be further tested with future exploration and analysis.

43

44 **Introduction**

45 Beginning with the acquisition of high-resolution images of the lunar surface from orbit, a
46 very wide and diverse array of morphologic features has been observed in association with the

47 lunar maria (e.g., flows, domes, cones, graben, sinuous rilles, ridges, pits, dark halo and mantle
48 deposits, etc.; Schultz, 1976; Wilhelms, 1987). Unclear has been the interpretation of each of
49 these features and how they might relate to specific eruption conditions and the range of
50 eruptions styles. We synthesize recent developments in understanding the origins and volatile
51 contents of lunar magmas, the mechanisms that transferred magma to the surface, and the factors
52 that controlled the eruption style of the resulting volcanism with emphasis on the effects of
53 volatile formation and release. We show how the specific influences of the physical
54 environment, especially the small value of the acceleration due to gravity and the negligible
55 atmospheric pressure, serve to combine with the nature and mode of volatile behavior to produce
56 the observed spectrum of lunar surface volcanic features.

57

58 **Constraints on lunar magmatism**

59 Lack of evidence for crustal contamination in lunar lava samples implies that most lunar
60 eruptions involved basaltic magma that passed rapidly from its mantle source to the surface
61 (Shearer et al., 2006). A model that readily explains this involves dikes nucleating at the tops of
62 ~500 km deep mantle partial melt zones (diapirs) when the slowly convectively-rising diapirs
63 encountered host rocks cool enough that the combination of host viscosity and diapir-imposed
64 strain rate exceeded the ability of the host rocks to deform plastically, so that a brittle fracture
65 nucleated (Wilson & Head, 2017a). Seepage of buoyant melt into the resulting crack caused the
66 slow (decades?) growth of a dike that, when a critical length of at least several tens of km was
67 reached, disconnected from the diapir source and migrated rapidly upward (a few hours) through
68 the mantle above it. The dike would have penetrated the low-density lunar crust to an extent
69 determined by the balance between the positive buoyancy of its lower part still in the mantle and
70 the negative buoyancy of its upper part in the crust. A few dikes penetrate to a shallow low-
71 density impact crater-related crustal zone and produce crater-contained sills known as floor-
72 fractured craters (Jozwiak et al., 2012, 2015) with consequent evolution of the intruded magma
73 (Wilson & Head, 2018). A sufficiently vertically extensive dike completely penetrating the crust
74 would break through to erupt at the surface. The great vertical extent of the dike meant that the
75 major lunar magmatic volatile, CO, was produced in amounts up to at least 1000 ppm by mass
76 over a wide range of depths in the dike, potentially extending down to at least 50 km in a large
77 enough dike. Additionally, up to at least 1000 ppm of water and sulfur compounds was released

78 in the upper few hundred meters of dikes (Rutherford et al., 2017). We explore the effects of this
79 behavior in the lunar environment.

80

81 **Distinctive characteristics of lunar volcanism**

82 The absence of an appreciable atmospheric pressure caused basaltic volcanic eruptions on the
83 Moon to have a vigorously explosive nature, despite the low magmatic volatile content by Earth
84 standards. This was especially true at the start of an eruption due to concentration of volatiles
85 into the upper parts of dikes approaching the surface (Wilson & Head, 2003). However, the
86 lunar versions of hawaiian and strombolian explosive activity differed greatly from those on
87 Earth (Wilson & Head, 1981), with no lunar analog of a convecting plinian eruption cloud (Head
88 & Wilson, 2017). The extreme expansion of even the smallest gas bubbles disrupted magma into
89 pyroclasts predominantly sub-mm in size. These clasts were accelerated by the expansion of the
90 released gases until the gas pressure became so low that the Knudsen regime was reached and the
91 interactions between gas and clasts became negligible; the clasts then continued on ballistic
92 trajectories until they reached the surface.

93 The giant 50-90 km long, 30-100 m wide dikes transferring magma volumes of up to ~1000
94 km³ to the lunar surface rose from the mantle at speeds of tens of m/s, and initially delivered
95 magma volume fluxes of up to ~10⁶ m³ s⁻¹ through the vents that they created to feed hawaiian-
96 style lava fountains (Wilson & Head, 2017a). The combination of high volume flux and small
97 pyroclast size caused many lunar lava fountains to be very optically dense, especially those with
98 relatively low volatile contents. Pyroclasts in the hot cores of such fountains were unable to
99 radiate heat into space and thus landed at magmatic temperature to coalesce into several hundred
100 km long lava flows that, having lost almost all of their gas, were nearly completely vesicle-free.
101 This condition continued as the rising dike decelerated toward buoyancy equilibrium and the
102 erupted volume flux decreased to ~10⁵ m³ s⁻¹. Once buoyancy equilibrium was achieved, the
103 erupted flux would have decreased to ~10⁴ m³ s⁻¹ as dike closure driven by lithospheric stresses
104 dominated the activity. Only when the volume flux decreased to less than ~3 × 10⁴ m³ s⁻¹ would
105 the lava fountain have begun to be optically transparent allowing extensive pyroclast cooling.
106 Long-lived eruptions of relatively volatile-poor magmas at these intermediate volume fluxes
107 were responsible for the thermo-mechanical erosion of the characteristic lunar sinuous rille
108 channels (Hurwitz et al., 2012). The relative duration of activity, and hence magma volumes

109 erupted, at these varying volume fluxes was a function of the vertical extent of the dike relative
110 to the thickness of the lunar crust. Figure 1 gives typical values.

111 Many lunar magmas appear to have released a few hundred ppm of mainly CO as they
112 erupted. In contrast, total magma volatile mass fractions of up to 3000 ppm (Rutherford et al.,
113 2017) in some picritic magmas led to pyroclast speeds in steady eruptions of up to 220 m/s and
114 maximum ranges of ~30 km. Greater speeds and ranges were possible in the initial stages of
115 eruptions as gas concentrated in the upper tips of dikes was released, and the combination of
116 these conditions produced extensive regional pyroclastic blankets (Head & Wilson, 2017).

117 Since all eruptions began with the arrival of a dike at the surface, initial vents were always
118 explosively erupting fissures, generally with lengths up to ~15 km (Head & Wilson, 2017). If the
119 fissure length was much less than the maximum range of the pyroclasts, gas effectively expanded
120 radially from a point source, producing a circular, umbrella-shaped fire fountain like those seen
121 on Io (Wilson & Head, 2001), though of very much smaller size (Head et al., 2002) due to the
122 much smaller volatile contents of the lunar magmas (Head & Wilson, 2017). If the fissure length
123 was comparable to or greater than the maximum pyroclast range, the fissure acted as a line
124 source and gas mainly expanded sideways away from the fissure, not radially. These differing
125 patterns of gas expansion and clast dispersal cause a concentration of clasts in the outer edges of
126 elongate fountains, enhancing their optical density. On the basis of these principles, we now
127 examine the stages in the evolution of a typical lunar mare basalt eruption to assess predictions
128 for resulting structures, landforms and volatile fate.

129

130 **Evolution of a typical lunar basaltic eruption: The four phases**

131 In order to link the ascent and eruption of magma to the observed landforms and structures,
132 we identify four stages in the evolution of a typical lunar eruption and examine how variations in
133 dike total volume, magma flux, gas content and eruption duration during each phase produce
134 different landforms (Figure 1).

135 *Phase 1 (Dike penetrates to surface, transient gas release phase)* is very explosive due to
136 volatile concentration into the low-pressure region near the upper tip of the propagating dike, but
137 is short-lived (Wilson & Head, 2003). In the extreme tip of the dike a zone of pure gas may
138 extend for 100-200 m, below which will be a foam layer with a high vesicularity extending
139 downward for ~10 km. Complete eruption of this gas-rich magma would have taken as little as 3

140 minutes and produced a very widespread but extremely thin deposit (Head & Wilson, 2017),
141 consistent with the ubiquitous volcanic glass beads found in soils even in the highlands.

142 *Phase 2 (Dike base still rising, high flux hawaiian eruptive phase)*, during which the dike as a
143 whole is still rising toward a neutral buoyancy configuration, has the highest magma discharge
144 rate $\sim 10^6 \text{ m}^3 \text{ s}^{-1}$, and involves the near-steady explosive eruption of magma with a volatile
145 content representative of the bulk of the magma. This would have involved the formation of a
146 relatively steady, largely optically dense hawaiian fire fountain within which sub-mm sized
147 pyroclastic droplets would have lost gas efficiently and accumulated with negligible cooling
148 within a few to 10 km of the fissure to form a vesicle-deficient lava lake. Lava would have
149 flowed away from the lake in an initially turbulent manner to form the distal part of the eventual
150 lava flow deposit in the case of a short lived eruption, or to feed a flow eroding a sinuous rille in
151 the case of a sufficiently long-lasting eruption (Figure 1). Given the relative vertical extents of
152 typical mantle dikes, $\sim 50\text{-}90 \text{ km}$ (Wilson & Head, 2017a), and the thickness of the lunar crust
153 ($\sim 30 \text{ km}$; Wicczorek et al., 2013), a significant part of the total dike magma volume would have
154 been erupted during this phase. Typically the duration of this phase would have been $\sim 5\text{-}10$
155 days, with erupted magma volume fluxes decreasing from $\sim 10^6 \text{ m}^3 \text{ s}^{-1}$ to $\sim 10^5 \text{ m}^3 \text{ s}^{-1}$ during this
156 period.

157 *Phase 3 (Dike equilibration, lower flux hawaiian to strombolian transition phase)* begins
158 when the dike feeding the eruption approaches an equilibrium, with the positive buoyancy of its
159 lower part in the mantle balancing the negative buoyancy of its upper part in the crust (Figure 1).
160 The lower dike tip then stops rising and the dike's vertical extent becomes fixed. The main
161 process driving this phase of the eruption is now the horizontal reduction in the thickness of the
162 dike as both its internal excess pressure, and the forced deformation of the host rocks by the
163 intrusion of the dike, relax (Wilson & Head, 2017a). While deformation of host rocks in the
164 shallow crust is probably elastic and rapid, deformation of hotter mantle rocks surrounding the
165 lower part of the dike is visco-elastic or viscous, resulting in a much longer time scale. During
166 this period, the vertical rise speed of the magma in the dike decreases greatly to less than 1 m s^{-1} ,
167 implying that the magma volume flux leaving the vent similarly decreases to a few $\times 10^4 \text{ m}^3 \text{ s}^{-1}$
168 over the course of 2-3 days. The reduced vertical magma flow speed means that gas bubbles
169 nucleating throughout the vertical extent of the dike can now rise at an appreciable rate through
170 the liquid, and there is time for larger bubbles, especially the CO bubbles being produced at great

171 depths, to overtake smaller bubbles leading to coalescence and even greater growth. This leads
172 to very large bubbles - gas slugs - filling almost all of the width of the dike and producing
173 strombolian explosions at the surface (Parfitt & Wilson, 1995). The change from hawaiian to
174 strombolian activity occurs quickly.

175 *Phase 4 (Dike closing, strombolian vesicular flow phase)* begins when the activity has
176 become entirely strombolian. Tectonic stresses continue to cause horizontal dike closure and
177 magma extrusion at a low flux. Magma from the deepest parts of the dike is still being forced
178 upward to lower pressure levels and so is continuing to produce some CO at all depths, and very
179 minor strombolian explosive activity continues above the vent as a result. However, a stable
180 crust forms on the magma still emerging from the vent and flowing away as lava.

181 There are two important potential consequences of Phase 4 activity. In some cases (Phase 4a,
182 low flux), this phase might begin only after most of the magma in the dike has already been
183 erupted and the volume flux has decreased to a very low level (Figure 1). This would be the case
184 for a dike that had a relatively small vertical extent, so that most of its magma was erupted while
185 the dike was still achieving equilibrium. The most likely consequence is then the emplacement
186 in the vicinity of the vent of vesicular lava as a series of cooling-limited flows superimposed on
187 earlier eruption products, in some cases building a small, low shield around the vent. The
188 magma being erupted now consists of liquid containing bubbles of a mixture of gases and
189 volatile elements (Gaillard and Scaillet, 2014; Renggli et al., 2017; Saal et al., 2018) defined by
190 the thermodynamic equilibrium between the products of interactions between mainly H₂O and
191 sulfur species released over the last <500 m of magma rise (Rutherford et al., 2017). These
192 bubbles would have nucleated with diameters of ~10-20 μm and would have grown to ~20-30
193 μm at the surface, remaining stable within the body of the lava as surface tension forces (Wilson
194 & Head, 2017b) imposed a retaining pressure of ~30 kPa. Lunar basalts exsolving ~1000 ppm of
195 these gases would have left the fissure vent as lava foams with vesicularities of more than 90%
196 by volume. Radiative cooling of the surface would have aided the stabilization of the bubbles at
197 the top surface of the foam, but would also have induced differential cooling stresses, and it is
198 likely that the top-most bubbles would have exploded into the overlying vacuum producing a
199 layer of bubble wall shards with sizes of ~10 μm. As long as gas could escape easily through
200 this accumulating debris layer, a wave of foam disintegration would have propagated downward
201 through the foam, increasing the thickness of the layer. However, this wave would rapidly have

202 reached depths where there had been no cooling, and so the disrupted bubble wall fragments
203 would have formed droplets that would have welded with one-another, forming a less vesicular
204 layer with some finite strength which, aided by the weight of the accumulated debris above,
205 would have inhibited further foam disintegration.

206 The weight of the overlying material would have determined the local pressure as a function
207 of depth and hence the depth down to which volatile exsolution could occur. The pressure at 1
208 meter depth in vesicular lava on Earth is typically 115 kPa whereas at that depth on the Moon the
209 value is ~1 kPa, one hundred times less. In general, therefore, Phase 4a low flux lava flows
210 would have consisted of a fragmental layer overlying a very vesicular layer. Collapse of such
211 flows could be consistent with the morphology of some of the irregular mare patches (IMPs)
212 documented by Braden et al. (2014) in the maria. If the flows are thick enough, these vesicular
213 layers could, in turn, overlie a layer of lava still containing dissolved volatiles. This as-yet
214 unvesiculated layer would become important as the lava cooled and crystallized if volatile
215 concentration into the remaining liquid caused second boiling and additional post-emplacement
216 vesiculation.

217 In other cases, with vertically more extensive dikes (Phase 4b, high flux), this phase might
218 commence with a large fraction of the total dike magma still being available for extrusion as
219 vesicular lava. In such cases this lava is likely to intrude into the still-hot interiors of the
220 previously-emplaced non-vesicular flows and cause them to inflate. A similar pattern of late-
221 stage magma intruding earlier-emplaced flow lobes is documented for flood-basalt lava fields on
222 Earth (Self et al., 1996). In the lunar case, the lower parts (<400 m depth) of the dike feeding
223 such intruding flows would contain water and sulfur compounds that had not yet been exsolved.
224 On a time-scale of weeks the resulting compound flows would cool, and the concentration of
225 volatiles into the residual liquid as crystallization occurred would lead to second boiling, with the
226 resulting new population of gas bubbles causing a further, possibly extensive, inflation episode.
227 Extrusion of the resulting magmatic foam through cracks in the lava crust may be an explanation
228 of the ring moat dome structures (RMDSs) (Zhang et al., 2017) found in large numbers on many
229 mare flows.

230 The total duration of Phase 4 of an eruption would have been controlled by the nature and
231 magnitude of the global stress state of the lithosphere, influencing visco-elastic relaxation of the
232 host rocks, and by cooling of the magma in the dike. Lunar thermal history (Solomon & Head,

233 1980) suggests that the lithosphere was under extensional stresses for the first ~1 Ga as
234 radiogenic heat accumulated and fed the onset of mare volcanism, followed at about 3.6 Ga by
235 compressive stresses as the interior cooled, encouraging faster closure of dikes in geologically
236 more recent eruptions. Dike models (Wilson & Head, 2017a) suggest that Phase 4 dikes would
237 have had initial widths of at least 10-20 m, and cooling of near-stagnant magma in such dikes by
238 conduction alone would require 1-2 years following the end of the eruption.

239

240 **Post-eruption changes in flows**

241 After the main phases of an eruption are complete and all motion has ceased, changes still
242 occur. Cooling of lava takes place at all boundaries, causing contractional stresses in the
243 thickening surface crust. Lava shrinks as its density increases, causing subsidence which is
244 greatest where lava has infilled pre-eruption depressions, thus adding differential stresses. These
245 can combine to form fractures in the cooled crust. Crystallization due to cooling increases the
246 concentration of residual volatiles in the remaining magmatic liquid causing supersaturation, and
247 second boiling leads to additional gas bubble nucleation. Where supersaturation and second
248 boiling occur in regions of a flow that already contain a foam core, expansion of the foam and
249 extrusion of foam through cracks onto the lava flow surface can occur.

250

251 **Consequences for observed volcanic features**

252 The volcanic features formed during these various phases of activity would have depended
253 critically on the vent configuration and the magma discharge rate and volatile content during the
254 various stages of the eruption. We identify nine different features typical of lunar volcanic
255 eruptions (Head & Wilson, 2017) and link them to the four eruptive phases described above.

256 *1. Pyroclastic mantles* form as the gas-rich tip of a dike initially reaches the surface and can
257 represent the products of Phase 1. All lunar eruptions should include such a phase, though the
258 deposit may be very thin and easily masked by regolith formation or subsequent volcanic activity
259 in low to moderate volatile content magmas. Additional pyroclasts can be dispersed around the
260 vent for hundreds of meters to several tens of km as magmatic volatile content varies during
261 Phase 2 hawaiian eruptions.

262 *2. Small shield volcanoes* consist of Phase 2 lavas erupted from dikes that have a relatively
263 small volume, so that neither the erupted volume nor the volume flux are large. Overflows from

264 the lava lake around the vent are fed at a low eruption volume flux and the resulting lava flows
265 do not travel far (~5-15 km) before stopping due to cooling. Previous flow deposits form
266 obstacles to subsequent lava outflows from the pond and so eventually flows will have left the
267 pond in all radial directions and a low shield volcano progressively accumulates. Subsequent
268 Phase 3/4 activity builds additional features at the summit of the volcano (strombolian spatter
269 and foam layers). Phase 4 (a) activity could also result in small, low shield volcanoes with
270 superposed foam layers and irregular mare patches, such as Cauchy 5 (Qiao et al., 2018).

271 3. *Compound flow fields* (Kreslavsky et al., 2017) form from relatively small-volume dikes
272 with low eruption fluxes. In contrast to small shield volcanoes that would form at central vents
273 on very low slopes, compound flow fields form from fissure eruptions on appreciable slopes.
274 Cooling limited flows induce multiple marginal breakouts upslope toward the vent, producing
275 the digitate map outline typical of compound flow fields.

276 4. *Sinuuous rilles and their source depressions* are initiated during Phase 2 eruptions from
277 dikes containing a large volume of low volatile content magma that erupts through a fissure less
278 than ~5 km long, ensuring a moderate volume flux. This generally creates a near-circular lava
279 pond that contains lava at magmatic temperature fed from an optically dense lava fountain. The
280 pond feeds a turbulent lava flow that efficiently erodes its substrate to form a sinuous channel
281 over the course of a few months as the eruption continues through phases 3 and 4.

282 5. *Long lava flows* represent Phase 2 eruptions from large-volume dikes that feed fissure vents
283 10-15 km long. The magma volatile content has little influence on the morphology of the distal
284 parts of the flow field emplaced from the early stages of the eruption because the high magma
285 volume flux guarantees an optically dense fire fountain forming a lava lake at magmatic
286 temperature, in turn feeding hot, turbulent volatile-free lava flows. However, the magma volatile
287 content becomes important later in Phases 3 and 4.

288 6. *Pyroclastic cones* form during Phases 3 and 4 of eruptions with an intermediate volatile
289 content. The change from steady to pulsating hawaiian activity, as the eruption progresses
290 towards the strombolian stage, allows the outer parts of the fire fountain to become partially
291 transparent so that partially cooled pyroclasts reach the ground to form spatter or cinder cones,
292 the degree of welding depending on the precise amount of cooling.

293 7. *Summit pit craters* can initially form from Phase 2 pyroclastic activity in low effusion rate,
294 small-shield building eruptions, with hawaiian pyroclast ranges out to ~0.5-1.5 km radius. They

295 may also be the result of Phase 4a activity from small-volume dikes erupting volatile-poor
296 magma from small shield summit vents, coupled with volume adjustments during late-stage
297 magma cooling. They also appear to commonly involve only short fissure vents, so that although
298 the low volatile content causes short pyroclast ranges, nevertheless a small and roughly circular
299 lava pond forms around the vent. In one case (Hyginus), escape of gas that has accumulated in
300 lateral dikes linked to the summit vent created a caldera (Wilson et al., 2011).

301 8. *Irregular mare patches (IMPs)* are interpreted to be related to Phase 4a activity from small-
302 volume dikes. After explosive activity becomes minimal, very vesicular magma from the dike is
303 emplaced under a cooling crust on the lava lake around the vent. In some cases this magmatic
304 foam breaks through the crust to form bulbous mounds that represent one class of IMP, as at the
305 small shield summit crater Ina (Qiao et al., 2017). In other cases the foam intrusion raises the
306 crust of the crater lake and overflows onto the upper flanks, where partial collapse of the foam
307 produces another type of IMP, such as those on the flanks of Cauchy 5 (Qiao et al., 2018).
308 Similar features occur on the floor of the Hyginus collapse caldera (Braden et al., 2014).

309 9. *Ring moat dome structures (RMDSs)* (Zhang et al., 2017) are interpreted to be the
310 consequence of Phase 4b activity from a large-volume dike. Earlier phases of the eruption
311 emplace long volatile-free lava flows. The Phase 4b activity injects partly-vesiculated lava into
312 the hot cores of the earlier flows causing inflation. Subsequent cooling and crystallization drives
313 exsolution of the remaining volatiles (second boiling), causing even more inflation and
314 producing large amounts of magmatic foam. Escape of the foam through cracks in the cooled
315 crust of the flow forms RMDSs. The moat surrounding the low dome structure is interpreted to
316 represent the consequence of the loading due to the extruded material coupled with conservation
317 of volume as the extrusion occurs.

318

319 **Conclusions**

320 We have used the basic principles of magma generation, ascent and eruption to examine the
321 range of dike volumes, effusion rates, volatile species and release patterns as a function of time
322 and eruption duration, subdividing eruptions into four sequential phases with specific individual
323 characteristics and predictions. These phases result in a unifying quantitative conceptual model
324 for the relationships among a wide and diverse range of related observed volcanic landforms and
325 structures such as pyroclastic mantles, small shield volcanoes, compound flow fields, sinuous

326 rilles and their source depressions, long lava flows, pyroclastic cones, summit pit craters,
327 irregular mare patches (IMPs), and ring moat dome structures (RMDSs). In contrast to viewing
328 the array of volcanic landforms each in isolation, these theoretical predictions provide the basis
329 for placing lunar volcanic landforms into eruptive sequences from individual eruptive events,
330 and linking them to potential variations in dike characteristics and evolution, effusion rates, and
331 volatile contents, that can provide clues to the nature of magma source regions. These
332 predictions and correlations can be further tested by future human and robotic lunar exploration
333 to specific destinations.

334

335 **Acknowledgements:** LW thanks the Leverhulme Trust for support through an Emeritus
336 Fellowship. We gratefully acknowledge funding to co-investigator JWH for participation in the
337 LOLA Experiment Team (Grants NNX11AK29G- National Aeronautics and Space
338 Administration and Goddard NNX13AO77G - National Aeronautics and Space Administration -
339 Goddard). Much of the synthesis work for this contribution was enabled by participation in the
340 NASA Solar System Exploration Research Virtual Institute, through the SEED (SSERVI
341 Evolution and Environment of Exploration Destinations) cooperative agreement number
342 NNA14AB01A at Brown University. Thanks are extended to Anne Côté for help in figure
343 drafting and preparation. We thank an anonymous reviewer for useful comments. No new data
344 were used in producing this manuscript.

345

346

347 **References**

- 348 Braden, S. E., Stopar, J. D., Robinson, M. S., Lawrence, S. J., van der Bogert, C. H., & Hiesinger,
349 H. (2014). Evidence for basaltic volcanism on the Moon within the past 100 million years.
350 *Nature Geoscience*, 7(11), 787–791. <https://doi.org/10.1038/NGEO2252>
- 351
- 352 Gaillard, F., & Scaillet, B. (2014) A theoretical framework for volcanic degassing chemistry in a
353 comparative planetology perspective and implications for planetary atmospheres. *Earth and*
354 *Planetary Science Letters*, 403, 307–316. <http://dx.doi.org/10.1016/j.epsl.2014.07.009>
- 355
- 356 Jozwiak, L. M., Head, J. W., Zuber, M. T., Smith, D. E., & Neumann, G. A. (2012), Lunar floor-
357 fractured craters: Classification, distribution, origin and implications for magmatism and
358 shallow crustal structure, *J. Geophys. Res.*, 117, E11005, doi: 10.1029/2012JE004134
- 360 Jozwiak, L. M., Head, J. W., & Wilson, L. (2015), Lunar floor-fractured craters as magmatic
361 intrusions: Geometry, modes of emplacement, associated tectonic and volcanic features, and
362 implications for gravity anomalies, *Icarus*, 248, 424-447, doi: 10.1016/j.icarus.2014.10.052
- 363
- 364 Head, J. W., & Wilson, L. (2017). Generation, ascent and eruption of magma on the Moon: New
365 insights into source depths, magma supply, intrusions and effusive/explosive eruptions (Part 2:
366 Observations). *Icarus*, 283, 176-223. <https://doi.org/10.1016/j.icarus.2016.05.031>

367

368 Head, J. W., Wilson, L., & Weitz, C. M. (2002). Dark ring in southwestern Orientale basin: origin
369 as a single pyroclastic eruption. *Journal of Geophysical Research - Planets*, 107(E1), 5001, 17
370 pp. <https://doi.org/10.1029/2000JE001438>
371

372 Hurwitz, D. M., Head, J. W., Wilson, L., & Hiesinger, H. (2012). Origin of lunar sinuous rilles:
373 modeling effects of gravity, surface slope, and lava composition on erosion rates during the
374 formation of Rima Prinz. *Journal of Geophysical Research - Planets*, 117, E00H14, 15 pp.
375 <https://doi.org/10.1029/2011JE004000>
376

377 Kreslavsky, M. A., Head, J. W., Neumann, G. A., Zuber, M. T. and Smith, D. E. (2017) Low-
378 amplitude topographic features and textures on the Moon: Initial results from detrended Lunar
379 Orbiter Laser Altimeter (LOLA) topography, *Icarus*, 283, 138-145, doi:
380 10.1016/j.icarus.2016.07.017
381

382 Parfitt, E. A., & Wilson, L. (1995). Explosive volcanic eruptions - IX: The transition between
383 Hawaiian-style lava fountaining and Strombolian explosive activity. *Geophysical Journal*
384 *International*, 121(1), 226-232.
385

386 Qiao, L., Head, J. W., Wilson, L., Xiao, L., Kreslavsky, M., & Dufek, J. (2017). Ina pit crater on
387 the Moon: extrusion of waning-stage lava lake magmatic foam results in extremely young
388 crater retention ages. *Geology*, 45(5), 455-458. <https://doi.org/10.1130/G38594.1>
389

390 Qiao, L., Head, J. W., Wilson, L., & Ling, Z. (2018). Lunar Irregular Mare Patch (IMP) sub-
391 types: Linking their origin through hybrid relationships displayed at Cauchy 5 small shield
392 volcano. *Lunar and Planetary Science XLIX*, abstract #1390.
393

394 Renggli, C. J., King, P. L., Henley, R. W., & Norman, M. D. (2017) Volcanic gas composition,
395 metal dispersion and deposition during explosive volcanic eruptions on the Moon. *Geochimica*
396 *et Cosmochimica Acta*, 206, 296-311. <http://dx.doi.org/10.1016/j.gca.2017.03.012>
397

398 Rutherford, M. J., Head, J. W., Saal, A. E., Hauri, E., & Wilson, L. (2017). Model for the origin,
399 ascent and eruption of lunar picritic magmas. *American Mineralogist*, 102, 2045-2053.
400 <https://doi.org/10.2138/am-2017-5994ccbyncnd>
401

402 Saal, A. E., Chaussidon, M., Gurenko, A. A., & Rutherford, M. (2018) Boron and Lithium
403 contents and isotopic composition of the lunar volcanic glasses. 49th Lunar and Planetary
404 Science Conference, Abstract #2575.
405

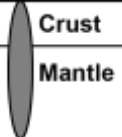
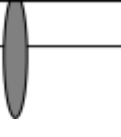

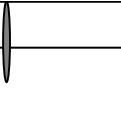
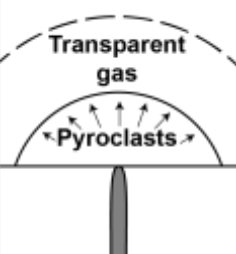
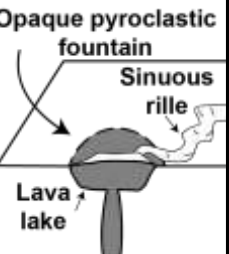
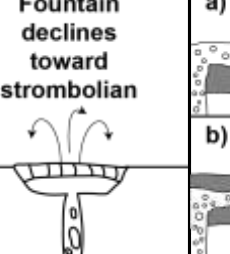
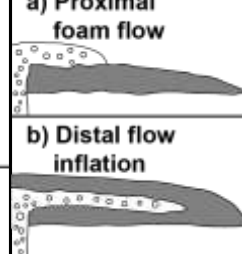
406 Self, S., Thordarson, Th., Keszthelyi, L., Walker, G. P. L., Hon, K., Muphy, M. T., Long, P., and
407 Finnemore, S. (1996). A new model for the emplacement of Columbia River basalts as large,
408 inflated pahoehoe lava fields. *Geophysical Research Letters*, 23(19), 2689-2692.
409

410 Shearer, C. K., Hess, P. C., Wieczorek, M. A., Pritchard, M. E., Parmentier, E. M., Borg, L. E. et
411 al. (2006). Thermal and magmatic evolution of the Moon. *Reviews in Mineralogy and*
412 *Geochemistry*, 60, 365-518. <https://doi.org/10.2138/rmg.2006.60.4>
413

- 414 Schultz, P. H. (1976) Moon Morphology: Interpretations Based on Lunar Orbiter Photography,
415 University of Texas Press, Austin, 626 pp.
416
- 417 Solomon, S. C., & Head, J. W. (1980). Lunar mascon basins: Lava filling, tectonics, and
418 evolution of the lithosphere. *Reviews of Geophysics and Space Physics*, 18, 107-141.
419
- 420 Wieczorek, M. A., Neumann, G. A., Nimmo, F., Kiefer, W. S., Taylor, G. J., Melosh, H. J., et al.
421 (2013). The crust of the Moon as seen on GRAIL. *Science*, 339, 671-675.
422 <https://doi.org/10.1126/science.1231530>
423
- 424 Wilhelms, D. E. (1987) The Geologic History of the Moon, U.S. Geological Survey Professional
425 Paper 1348, 302 pp.
426
- 427 Wilson, L., & Head, J. W. (1981). Ascent and eruption of basaltic magma on the Earth and Moon.
428 *Journal of Geophysical Research*, 86, 2971-3001.
429
- 430 Wilson, L., & Head, J. W. (2001). Lava fountains from the 1999 Tvashtar Catena fissure eruption
431 on Io: implications for dike emplacement mechanisms, eruption rates and crustal structure.
432 *Journal of Geophysical Research - Planets*, 106(E12), 32,997-33,004.
433
- 434 Wilson, L., & Head, J. W. (2003). Deep generation of magmatic gas on the Moon and
435 implications for pyroclastic eruptions. *Geophysical Research Letters*, 30(12), 1605, 4 pp.
436 <https://doi.org/10.1029/2002GL016082>
437
- 438 Wilson, L., & Head, J. W. (2017a). Generation, ascent and eruption of magma on the Moon: New
439 insights into source depths, magma supply, intrusions and effusive/explosive eruptions (Part 1:
440 Theory). *Icarus*, 283, 146-175. <https://doi.org/10.1016/j.icarus.2015.12.039>
441
- 442 Wilson, L., & Head, J. W. (2017b). Eruption of magmatic foams on the Moon: Formation in the
443 waning stages of dike emplacement events as an explanation of “Irregular Mare Patches”.
444 *Journal of Volcanology and Geothermal Research*, 335, 113-127.
445 <https://doi.org/10.1016/j.volgeores.2017.02.009>
446
- 447 Wilson, L., & Head, J. W. (2018) Lunar floor-fractured craters: Modes of dike and sill
448 emplacement and implications of gas production and intrusion cooling on surface morphology
449 and structure, *Icarus*, 305, 105-122, doi: 10.1016/j.icarus.2017.12.030
450
- 451 Wilson, L., Hawke, B. R., Giguere, T. A., & Petrycki, E. R. (2011). An igneous origin for Rima
452 Hyginus and Hyginus Crater on the Moon. *Icarus*, 215(2), 584-595.
453 <https://doi.org/10.1016/j.icarus.2011.07.003>
454
- 455 Zhang, F., Head, J. W., Basilevsky, A. T., Bugiolacchi, R., Komatsu, G., Wilson, L., Fa, W., &
456 Zhu, M.-H. (2017). Newly-discovered ring-moat dome structures in the lunar maria: possible
457 origins and implications. *Geophysical Research Letters*, 44(18), 9216-9224.
458 <https://doi.org/10.1002/2017GL074416>
459

460
 461
 462
 463
 464

Figure 1. The characteristics of the four eruption phases during a typical lunar eruption, with diagrams and parameters representing average values. The relative duration of individual phases depends on the total dike volume and vertical extent.

Eruption Phase	PHASE 1	PHASE 2	PHASE 3	PHASE 4
	Dike penetrates to surface, transient gas release phase	Dike base still rising, high flux hawaiian eruptive phase	Dike equilibration, lower flux hawaiian to strombolian transition phase	Dike closing, strombolian vesicular flow phase
Dike Configuration				
Surface Eruption Style				
Magma Rise Speed	30 to 20 m/s	20 to 10 m/s	5 to <1 m/s	< 1 m/s
Magma Volume Flux	$\sim 10^6$ m ³ /s	10^6 to 10^5 m ³ /s	10^5 to $\sim 10^4$ m ³ /s	$\sim 10^4$ m ³ /s
Percent Dike Volume Erupted	<5%	$\sim 30\%$	$\sim 30\%$	$\sim 35\%$
Phase Duration	~ 3 minutes	5-10 days	2-3 days	10-100 days
Flow Advance Rate	n/a	~ 3 to 0.1 m/s	0.03 m/s	0.01 m/s
Flow Advance Distance	n/a	300 km	305 km	335 km
Vesicularity of Flow	n/a	zero	low, but increasing	very high

465